







Coulomb-free 1S_0 $p-p$ scattering length from the quasi-free $p+d \rightarrow p+p+n$ reaction and its relation to universality

Aurora Tumino^{1,2}[✉], Giuseppe G. Rapisarda^{2,3}, Marco La Cognata², Alessandro Oliva^{2,3}, Alejandro Kievsky⁴, Carlos A. Bertulani⁵, Giuseppe D'Agata², Mario Gattobigio⁶, Giovanni L. Guardo², Livio Lamia^{2,3,7}, Dario Lattuada^{1,2}, Rosario G. Pizzone², Stefano Romano^{2,3,7}, Maria L. Sergi^{2,3}, Roberta Spartá² & Michele Viviani⁴

The Coulomb-free 1S_0 proton-proton ($p-p$) scattering length relies heavily on numerous and distinct theoretical techniques to remove the Coulomb contribution. Here, it has been determined from the half-off-the-energy-shell $p-p$ scattering cross section measured at center-of-mass energies below 1 MeV using the quasi-free $p+d \rightarrow p+p+n$ reaction. A Bayesian data-fitting approach using the expression of the s -wave nucleon-nucleon scattering cross section returned a $p-p$ scattering length $a_{pp} = -18.17^{+0.52}_{-0.58}|_{stat} \pm 0.01|_{syst}$ fm and effective range $r_0 = 2.80 \pm 0.05|_{stat} \pm 0.001|_{syst}$ fm. A model based on universality concepts has been developed to interpret this result. It accounts for the short-range interaction as a whole, nuclear and residual electromagnetic, according to what the s -wave phase-shift δ does in the description of low-energy nucleon-nucleon scattering data. We conclude that our parameters are representative of the short-range physics and propose to assess the charge symmetry breaking of the short-range interaction instead of just the nuclear interaction. This is consistent with the current understanding that the charge dependence of nuclear forces is due to different masses of up-down quarks and their electromagnetic interactions. This achievement suggests that these properties have a lesser than expected impact in the context of the charge symmetry breaking.

¹Facoltà di Ingegneria e Architettura, Università degli Studi di Enna "Kore", Enna, Italy. ²INFN-Laboratori Nazionali del Sud, Catania, Italy. ³Dipartimento di Fisica e Astronomia "Ettore Majorana", Università degli Studi di Catania, Catania, Italy. ⁴INFN-Sezione di Pisa, Pisa, Italy. ⁵Department of Physics and Astronomy, Texas A&M University-Commerce, Commerce, TX 75429, USA. ⁶Université Côte d'Azur, CNRS, Institut de Physique de Nice, 06560 Valbonne, France. ⁷Centro Siciliano di Fisica Nucleare e Struttura della Materia, Catania, Italy. ✉email: tumino@lns.infn.it

The longstanding hypothesis of charge independence and charge symmetry of nuclear forces can be unveiled by fixing the low energy parameters of the strong nucleon-nucleon (NN) interaction in the spin-singlet 1S_0 state¹. Charge independence requires that nuclear forces do not distinguish between neutron and proton, while charge symmetry relies on the same interaction between two neutrons and two protons. Violation of the first one is associated with the mass difference between charged and neutral pions, responsible for the different values of the nuclear force range between two neutrons (or two protons) and neutron-proton. Indeed, while identical nucleons exchange a neutral pion, a neutron and a proton may exchange both a neutral and a charged pion. The charge symmetry breaking is mainly attributed to the up-down quark mass difference, though its validity is supported to some extent by an approximate equality of binding energies of isobar nuclei. The charge symmetry breaking of the nucleon-nucleon interaction seems to be manifested in the s -wave scattering lengths that determine the low-energy behavior of NN scattering¹.

A precise determination of the s -wave scattering lengths for neutron-proton (n - p), proton-proton (p - p), and neutron-neutron (n - n) interactions can provide important hints to definitively solve this problem. Moreover, these parameters are fundamental quantities in developing the nuclear-force models to explore the nuclear structure/properties and the interactions between nuclei.

The n - p scattering length is the only one directly determined from experiments, since the Coulomb effects need to be theoretically removed from experimental p - p data to reveal the strong interaction contribution to the scattering length, while it is impossible to study the n - n scattering directly because of the absence of neutron targets². The knowledge of these quantities, however, will help to distinguish between the n - n and p - p interactions. In the framework of the chiral effective field theory, such differences between the two interactions would appear at the fourth order (N³LO). As for the p - p scattering, the accurate and numerous experiments performed so far throughout a broad energy range, have revealed that Coulomb corrections are large. One of the latest estimates of the uncorrected p - p scattering length using available p - p scattering world data at p laboratory energies below 30 MeV is quoted as -7.8063 ± 0.0026 fm³. The p - p scattering length for switching off the Coulomb interaction is different from it because the phase shifts are non-linear functions of the interactions. The removal of electromagnetic interactions requires sophisticated theoretical tools, which, although fairly well assessed, can introduce considerable model dependence and some uncontrolled systematic uncertainty in the nuclear p - p scattering length thus derived⁴⁻⁶. Some of them invoke, for example, effective field theory expansions^{7,8} including short-distance effects of the Coulomb potential⁹, or heavy-baryon chiral perturbation theories¹⁰. The outcome can be as low as -14.9 ± 0.3 fm⁸ or up to values ranging from -16.0 ± 0.3 fm¹¹ to -17.5 ± 0.3 fm¹⁰. The scatter of about 2.5 fm between the corrected values can be hazarded as an estimate of the systematic uncertainty coming from theory. Moreover, by comparing the relative uncertainties before and after the correction, we can conclude that though still very low, the model corrections bring an increase in the relative uncertainty of almost two orders of magnitude.

The present situation is outlined in Ref. 12: from the vast body of experimental data obtained so far, the current accepted values for the n - p , nuclear p - p and n - n scatterings are $a_{np} = -23.74 \pm 0.02$ fm, $a_{pp}^N = -17.3 \pm 0.4$ fm and $a_{nn}^N = -18.9 \pm 0.4$ fm.

However, it should be pointed out that the determination of the nuclear scattering length introduces a model dependence due to the arbitrary exclusion of the short-range electromagnetic contributions. A well defined, almost model-independent quantity would be the short-range scattering length. For the pp system,

this would require that only the long-range Coulomb contribution is subtracted but all the short-range contributions are taken into account. In the present work, and to our knowledge for the first time, we determine the Coulomb free p - p scattering length and effective range taking advantage of the half-off-the-energy-shell (HOES) p - p scattering obtained by measuring the $^2\text{H}(p, pp)n$ reaction in quasi-free kinematics with the Trojan Horse Method (THM)^{13,14}. At the same time, we develop an almost model-independent procedure to extract the Coulomb free p - p parameters from their direct p - p experimental values. This procedure is based on universal concepts thanks to the particular location of the two-nucleon system inside the universal window, a region of the interaction parameters characterized by the presence of a shallow state (bound or virtual). The presence of this soft scale is well suited for a description based on the effective field theory framework¹⁵ as the various quantities become insensitive to the details of the nuclear potential models. It is exploiting this fact that our theoretical analysis becomes almost model-independent.

Results and discussion

Coulomb-free p - p scattering cross section. The primary ingredient of the present work, i.e. the HOES p - p scattering cross section, is the result of a measurement of the $^2\text{H}(p, pp)n$ reaction in quasi-free kinematics with the THM^{13,14}. The THM is a well known indirect technique, which has its roots in the unique properties of the quasi-free mechanism^{16,17} that allows to study reactions between charged particles at sub-Coulomb energies free of Coulomb suppression as well as electron screening (see “THM basic features” in the Methods section). In particular, the aim of the $^2\text{H}(p, pp)n$ measurement was to investigate the restraint of the Coulomb amplitude. A striking application of the THM where this restraint can be observed is exactly the p - p scattering at low energy, whose excitation function beautifully displays a deep minimum ($E_{pp} = 191.2$ keV, $\theta_{cm} = 90^\circ$). This minimum is a direct signature of the interference between nuclear and Coulomb scattering amplitudes. Indeed, an evidence of a vanishingly small Coulomb contribution is the lack of the interference minimum in the HOES p - p scattering excitation function. An exhaustive description of the experimental measurement as well as of data analysis performed in plane wave impulse approximation (PWIA) is given in^{13,14}. Here we will recall the basic features needed for the purpose of the present work.

We recall the compelling agreement between experimental THM p - p scattering data, shown in Fig. 1 as red solid circles and the independently calculated HOES behavior based on the formalism developed in¹⁴ displayed as black solid line in the same figure.

The formalism yields:

$$\left(\frac{d\sigma}{d\Omega_{c.m.}}\right)^{HOES} = \frac{1}{4k^2} \left(|F(\mathbf{p}, \mathbf{k}) - 2T_{CN}(p, k)|^2 + 3|F(\mathbf{p}, \mathbf{k})|^2 \right), \quad (1)$$

where

$$F(\mathbf{p}, \mathbf{k}) = m_p e^2 e^{-\pi\eta} \Gamma(1 + i\eta) (p^2 - k^2)^{i\eta} g(\mathbf{p}, \mathbf{k}),$$

with

$$g(\mathbf{p}, \mathbf{k}) = (\mathbf{p} - \mathbf{k})^{-2(1+i\eta)} \pm (\mathbf{p} + \mathbf{k})^{-2(1+i\eta)},$$

the \pm sign depending on whether the total spin of the two protons is $S = 0$ (singlet state, first term in the brackets in Eq. (1)) or $S = 1$ (triplet state, second term in the brackets in Eq. (1)), respectively. Here, $p(k)$ is the relative off-shell(on-shell) momentum of the protons in the incoming(outgoing) channel, e is the electric charge, m_p the proton mass and η the Sommerfeld parameter. The Coulomb-modified nuclear HOES p - p scattering amplitude,

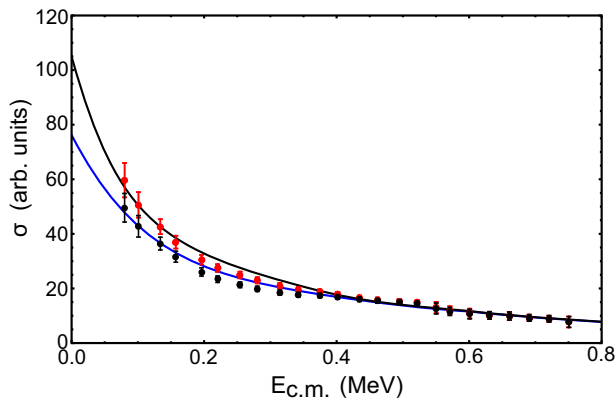


Fig. 1 Coulomb-free p - p scattering cross section. HOES p - p scattering cross section from a weighted average of all the experimental data reported in¹⁴ versus the relative p - p kinetic energy (red solid circles). The black solid line represents the theoretical HOES p - p cross section obtained using Eq. (1). The blue solid line refers to the same Eq. (1) with the two proton charges Ze set to zero so as to turn off the residual Coulomb interaction. Black solid circles represent the HOES p - p scattering cross section after removal of the residual Coulomb interaction (see text for details). Error bars denote $\pm 1\sigma$ uncertainties.

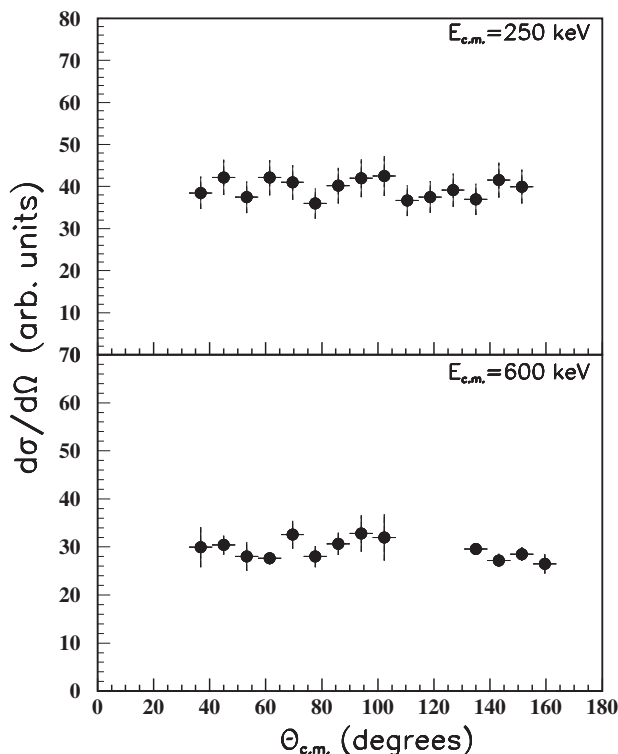


Fig. 2 Experimental proton angular distributions. Results are shown as black solid circles and refer to p - p relative energies of $E_{cm} = 250$ keV and $E_{cm} = 600$ keV. Error bars indicate $\pm 1\sigma$ uncertainties.

T_{CN} , at low energies can be also written in analytical form¹⁴. This expression predicts a drastic suppression of the Coulomb interaction in quasi-free scattering. It only accounts for the s partial wave since for the elastic scattering at sub-Coulomb energies the s wave gives overwhelming contribution also to the HOES scattering cross sections, due to the fast decreasing of the scattering phase shifts for $l > 0$. This is reflected in the isotropic behaviour of the experimental p angular distributions, as shown

in Fig. 2 for p - p relative energies of 250 and 600 keV. The reported center-of-mass angle is the one between the momentum of any of the two protons and the beam direction¹⁸. The fact that the calculated HOES p - p cross section nicely fits the THM data is a proof of validity of the PWIA factorization (see “THM basic features” in the Methods section) of the ${}^2\text{H}(p, pp)n$ cross section.

As noticed in Ref. 14, THM data below a p - p center of mass energy of 200 keV show a slight increase with respect to the nuclear on-the-energy-shell (OES) p - p behavior, due to a residual Coulomb interaction in the T_{CN} term. This residual contribution disappears from the HOES treatment by replacing the two proton charges Ze by zero, fairly reproducing the behavior of the calculated n - n and pure nuclear p - p cross sections as given in¹⁹. The solid blue line in Fig. 11(b) of Ref. 14 clearly displays the success of using this procedure, where the model uncertainty is smaller than the statistical error. We will refer to this line as the HOESn p - p cross section. To determine the Coulomb free p - p scattering cross section from the ${}^2\text{H}(p, pp)n$ data, the residual Coulomb interaction has been removed dividing the extracted p - p cross section by a correction term obtained from the ratio between the theoretical HOES p - p and HOESn p - p cross sections. The result is reported in Fig. 1 as black solid circles, with the solid blue line representing the HOESn p - p cross section. This procedure introduces a negligible uncertainty (less than 0.5%), quoted through the analysis of the covariance matrix. This is a clear effect of the correlation between HOES and HOESn curves originating from the same Eq. (1) and represents indeed an advantage of the methodology.

Scattering length and effective range from a Bayesian approach analysis. The p - p scattering data free of residual Coulomb interaction were fitted with the s -wave effective-range expansion, the conventional tool to analyze NN scattering data at low energies^{19–22}. For the low energy NN s -wave phase shift, δ , it reads

$$k \cot \delta = -\frac{1}{a} + \frac{1}{2} r_0 k^2, \quad (2)$$

where k denotes the relative momentum of the NN pair and a and r_0 are the scattering length and the effective range parameters, respectively.

The s -wave NN scattering cross section is given by

$$\sigma_{tot} = \frac{4\pi}{\left(\frac{1}{a} - \frac{1}{2} r_0 k^2\right)^2 + k^2}. \quad (3)$$

The fit was done with three free parameters: a , r_0 and a normalization coefficient C . The latter was introduced to remove the possible systematic uncertainty coming from the data normalization procedure of^{13,14}, which however is less than 2%. The quasi-free p - p scattering cross section deduced from the ${}^2\text{H}(p, pp)n$ data using the THM, is indeed not normalized^{13,14}. An overall normalization was done in^{13,14} by matching to the theoretical on-shell p - p cross-section above the Coulomb barrier after being averaged out at the same energy bin of THM data. Here, a Bayesian approach (see Methods section “Bayesian analysis approach”) was used to fit the data, in order to better sample the parameters of the cross section model (Eq. (3)) according to our data. A Markov Chain Monte Carlo (MCMC) was implemented using the *emcee* Python library²³, which is based on the algorithm described in²⁴. A flat prior distribution was chosen for a , sampled in the interval (-25 fm, -15 fm) to account for the large historical dispersion of this model parameter. A Gaussian prior distribution was taken for r_0 with centroid at 2.80 fm corresponding to the weighted average of the current accepted values from the three NN combinations and $\sigma = 0.04$ fm. A Gaussian prior distribution was taken for the

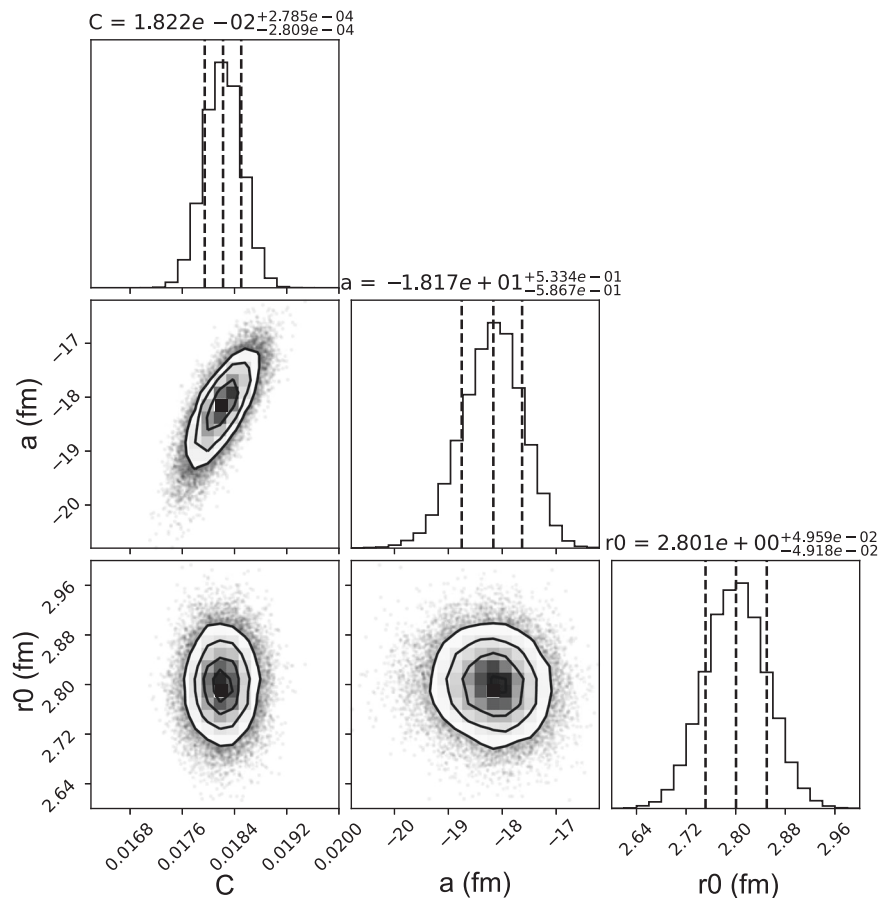


Fig. 3 Corner plot from the Bayesian approach analysis. Corner plot of the posterior distributions from the MCMC analysis for a , r_0 and C model parameters. The level-like curves in the two-dimensional plots display from inside to outside the 1σ , 2σ 3σ confidence intervals of the posterior distributions for the three parameters. The 1σ range is also highlighted by the dashed lines in the one-dimensional plots.

normalization coefficient C as well, having found that it varies within few percents throughout the intervals chosen for the model parameters. The result of the fit is shown in Fig. 3 with the final posterior distribution from the MCMC analysis. The small correlation observed between C and a_{pp} is expected as normalization shifts the fitting line and, more importantly, its intercept. The overall systematic uncertainties amount to a 2% and result from the normalization procedure (1.5%) and from the subtraction of the FSI contribution in the selected region of events with neutron momentum values lower than 20 MeV/c (1.4%) as reported in^{13,14}. These two uncertainties have been combined in quadrature. Separating the statistical uncertainties from the systematic ones, the numbers read as: $a_{pp} = -18.17^{+0.52}_{-0.58}|_{stat} \pm 0.01|_{syst}$ fm and $r_0 = 2.80 \pm 0.05|_{stat} \pm 0.001|_{syst}$ fm. Consistent numbers result from individual fits of the single data sets from the independent measurements reported in Fig. 10 of^{13,14}.

The result of the fit is shown in the upper panel of Fig. 4 as solid black line with Coulomb free THM p - p scattering data given as black solid circles. Dotted red, blue and black lines in the same figure refer to Eq. (3) with current accepted values for nuclear a and r_0 parameters from n - n , p - p and n - p scatterings, respectively. The residuals of the THM data about the fitting line are shown in the bottom panel of Fig. 4 as black solid circles. The dashed black lines in the panel are obtained accounting for the errors in the fitting parameters. Residuals help to better visualize the good quality of the fitting procedure, with all the points touching with the error bars the dashed black lines.

Numbers from our results and current accepted values for nuclear n - p , p - p and n - n scatterings (with upper case N) are

reported in Table 1 for a better comparison. The a_{np}^N value is taken from²⁵. It turns out that our extracted a_{pp} value from the quasi free p - p scattering, while disagreeing with a_{np}^N , barely agrees within experimental errors with the world accepted a_{pp}^N value, and sits closer to the a_{nn}^N estimate. This observation deserves further consideration. Despite being in a very low-energy region where the interacting protons appear as point-like, the NN s -wave phase shift δ of eq. (2) contains all short range effects, including the electromagnetic ones. This means that the present analysis of the HOES cross section allows direct access to the short-range p - p interaction as a whole, with its peculiar a_{pp} and r_0 values. A different comparison with the corresponding literature value from the short range physics⁵ would therefore be more appropriate. Universal concepts can be exploited in this context to better interpret the results. In fact, the suppression of Coulomb effects places the p - p system to the same level as the n - p and n - n systems, thus allowing to apply the concept of universal window to perform a particular analysis of these low energy parameters.

The universal window. The universal (or unitary) window is a region characterized by the presence of a very shallow state with energy close to threshold. At the same time the two-body scattering length a reaches values close to infinity. When a is large, the two-body shallow state can be real ($a > 0$) or virtual ($a < 0$) with its energy governed by the scattering length, $E \approx \hbar^2/ma^2$. Its shallow character emerges by comparing its energy to a typical energy of the system, $\hbar^2/m\ell^2$, where ℓ could be a typical length,

for example the interaction range. When $\ell/a \ll 1$, the system is inside the unitary window. Notably, in this particular region, universal behavior can be observed, the dynamics being largely independent of the details of the interaction. It is dominated by the long-range behavior allowing for a description based on few parameters. Universal behavior can be observed in very different systems as nuclear, atomic or hadron physics²⁶. Nuclear physics is a remarkable example; in the $S = 1$ spin channel, the deuteron binding energy is $E = 2.22456$ MeV, a value much smaller than the typical nuclear energy $\hbar^2/2m\ell^2 \approx 10$ MeV, where we have estimated the interaction range $\ell \approx 1.4$ fm. The $S = 0$ spin channel is particularly interesting, with the very large (and negative) $n - p$ and $n - n$ scattering lengths implying the existence of very shallow virtual states. In the $p - p$ case, the presence of the Coulomb force slightly modifies this analysis. However, it is possible to extract the corresponding scattering length and effective range values as produced by the short-range interaction only. In the paragraph “Effective Field Theory Concepts” of the Methods section, an almost model independent procedure is introduced to extract the low-energy parameters as produced by the short-range physics. The procedure is based on the

low-energy effective range expansion (Eq. (2)) and using the S -matrix pole equation $k \cot \delta = ik$, its extension to the imaginary axis, $k = i\kappa$, relates the shallow energy pole to the scattering parameters:

$$\frac{1}{a_B} = \frac{1}{a} + \frac{1}{2} \frac{r_0}{a_B^2}, \quad (4)$$

here $E = \hbar^2 \kappa^2 / m = \hbar^2 / m a_B^2$ defines the energy length a_B . These two equations, which are simultaneously verified inside the universal window, introduce a strict correlation (valid up to second order) between the low-energy parameters allowing for an effective description of the dynamics in terms of the long-range physics. This will be achieved in the next section by using a two-parameter potential, as for example a Gaussian, with the parameters fixed to match the long range behavior. To some extent this treatment is equivalent to a next-to-leading order description in the effective field theory framework. It should be pointed out that Eq. (4) is verified when the shape parameters, i.e. those parameters proportional to the k^4 and higher terms in the effective range expansion, produce almost a negligible contribution. For example, using experimental values, in the case of the $S = 1$ channel, Eq. (4) is verified at the level of 0.1% whereas it is even better verified in the $S = 0$ case.

Effective description. Taking advantage of the properties of the universal window, we develop a model to account for the short-range interaction of the two protons. We start from observing that literature values of the singlet effective range r_0 for pp , np and nn are compatible with a single value around 2.8 fm. This observation has guided the choice of the r_0 prior distribution in the Bayesian fit and here is used to construct a two-parameter Gaussian NN interaction with fixed range, valid for s-wave in the spin singlet channel (see Methods section “Effective Field Theory Concepts”),

$$V_{NN}(r) = V_0 e^{-r^2/r_G^2} + \frac{e_{NN}^2}{r}, \quad (5)$$

with $NN \equiv nn, np, pp$ and $e_{pp}^2 = e^2$ and zero otherwise. By varying the strength V_0 , this interaction is well suited to characterize the universal window in the region where the NN 0^+ systems are located (see Methods section). Let us stress that the Gaussian form selected to represent the short-range interaction is not relevant, other choices are acceptable as well. Forms that in some limit reduce to a contact interaction are equivalent for the purpose of the present analysis. In fact, as discussed in recent times, the low-energy dynamics of the two-nucleon system shows a large independence of the interaction details²⁷. With reference thereto, an exercise with the Argonne v_{18} NN potential²⁵ used to produce reference values is performed in the Methods section under “Effective Field Theory Concepts” to show the advantages of working in the universal window. Specifically, to characterize the 0^+ NN systems, we use a Gaussian range value of $r_G = 1.85 \pm 0.05$ fm. We first vary the strength V_0 to describe the experimental a_{nn} , a_{np} short-range values¹², given in the sixth column of

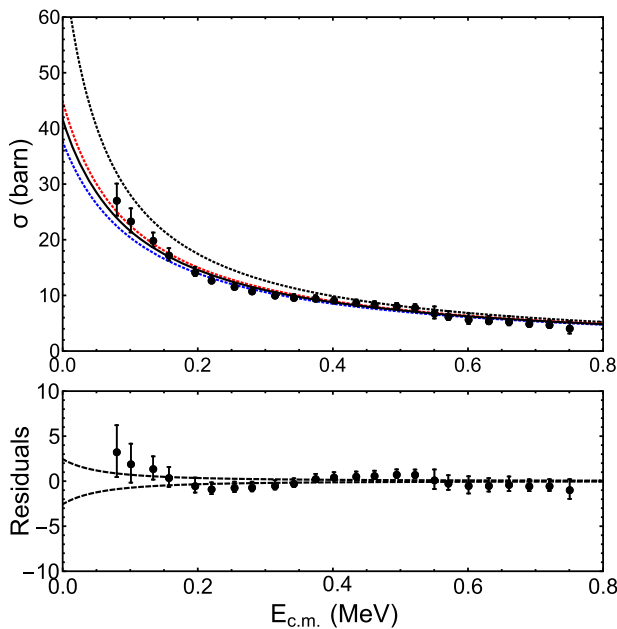


Fig. 4 Results of the Bayesian fit on the Coulomb-free p - p scattering cross section. Upper panel: Experimental quasi-free p - p scattering cross section after removal of the residual Coulomb interaction (black solid circles). Error bars indicate $\pm 1\sigma$ uncertainties. The result of the fit using Eq. (3) is shown as solid black line, while the dotted red, blue and black lines refer to Eq. (3) for n - n , p - p and n - p scatterings, respectively, using current accepted values for nuclear a and r_0 parameters. Lower panel: residuals of black solid circles in the upper panel to the solid black line. The dashed black lines are obtained accounting for the errors in the fitting parameters.

Table 1 Numbers of low energy parameters.

NN	$a^N(\text{fm})$	$r_0^N(\text{fm})$	$a^{\text{THM}}(\text{fm})$	$r_0^{\text{THM}}(\text{fm})$	$a^{\text{sr}}(\text{fm})$	$r_0^{\text{sr}}(\text{fm})$	$V_0(\text{MeV})$
np	-23.08 ± 0.02	2.77 ± 0.05			-23.74 ± 0.02	2.80 ± 0.08	-29.90
pp	-17.3 ± 0.4	2.85 ± 0.04	$-18.17^{+0.53}_{-0.59}$ fm	2.80 ± 0.05 fm	-17.6 ± 0.4	2.85 ± 0.09	-29.08
nn	-18.9 ± 0.4	2.75 ± 0.11			-18.6 ± 0.4	2.85 ± 0.08	-29.22

Current accepted values of a and r_0 parameters, (N superscript stands for “nuclear”) for n - p , p - p and n - n scattering compared with those obtained in this work (“THM” superscript). In the last three columns, the values and the corresponding strength V_0 obtained with the Gaussian characterization are given. The sr superscript stands for “short-range” (nuclear + EM).

Table 1, second and fourth row, as a_{nn}^{sr} and a_{np}^{sr} respectively. Note that using $r_G = 1.85 \pm 0.05$ fm, the effective ranges r_{nn}^{sr} , r_{np}^{sr} take on values close to the experimental data. The results for these quantities and the corresponding strength V_0 are given in the last two columns of Table 1, second and fourth row. In each case the calculation has been done with the corresponding reduced mass.

To analyze the pp case, we consider the Coulomb interaction and fix the strength V_0 to describe the experimental a_{pp} value of $-7.8063(26)$ fm. Then, we calculate the corresponding value without the Coulomb term obtaining -17.6 fm fairly similar to the one from⁵ calculated using the Paris potential. We consider this value an estimate of the pp scattering length a_{pp}^{sr} coming from the short-range physics and quote in Table 1, sixth column, third row. Moreover, considering a variation of the Gaussian range $r_G = 1.85 \pm 0.05$ fm we assign an error to the short-range pp scattering length as $a_{pp}^{sr} = -17.6 \pm 0.4$ fm. All theoretical uncertainties reported in Table 1 have been calculated in this way.

It should be stressed that the value $a_{pp}^{sr} = -17.6 \pm 0.4$ fm results from considering the short-range physics, nuclear and electromagnetic, as the Gaussian interaction captures the short-range contributions. A comparison with the THM estimate is therefore appropriate, providing agreement within experimental errors. It is amazing how the simple concept of universality supports the experimental result. The situation is illustrated in Fig. 5, in which the different NN systems are located inside the universal window in terms of the coordinates $[x, y] = [r_0/a_B, r_0/a]$ as given by the above analysis. Interestingly, they lie on the curve $y = x - 0.5x^2$ verifying the correlation imposed by Eq. (4). The 0^+ and 1^+np systems are well determined by the corresponding experimental values, and they have a precise position along the $y(x)$ curve. Conversely, the 0^+nn and pp systems suffer from some historical indeterminations due to difficulties in the measurements (the nn system) or, in the pp case, the model dependence introduced to discriminate between the nuclear and the electromagnetic short-range contributions. Using the property highlighted here that the systems move along the universal curve, it is possible to reduce the model dependence in the determination of the scattering parameters as produced by the short-range part of the interaction without discriminating between nuclear and electromagnetic.

A new paradigm is thus proposed: to address the problem of charge symmetry breaking taking into account the short range effects as a whole now that the first Coulomb-free $p-p$ scattering data at low energy are available. This would remove the largest

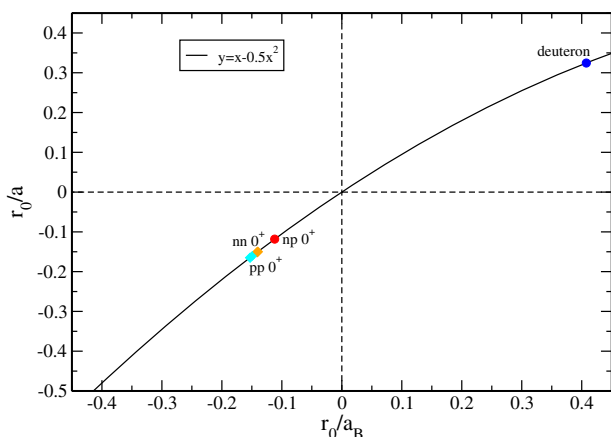


Fig. 5 Predictions for the NN systems inside the universal window. The positions of the NN systems on the universal curve as deduced from the effective description are clearly displayed. Their coordinates $[x, y] = [r_0/a_B, r_0/a]$ are related to the scattering parameters produced by the short-range physics.

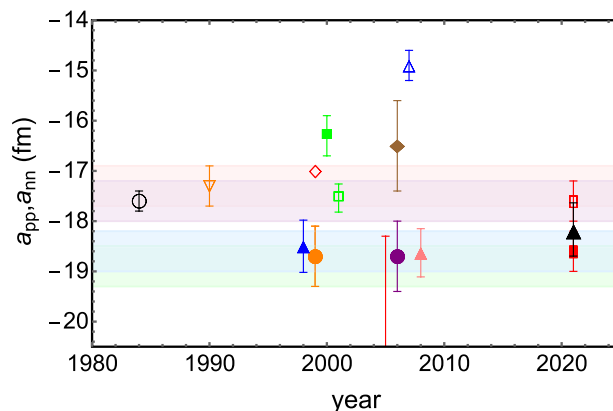


Fig. 6 Present a_{pp} results in the context of recent literature. Present THM a_{pp} value (black triangle) and a_{nn}^{sr} (filled red rectangle) and a_{pp}^{sr} (empty red rectangle) from the Gaussian model, are compared with recent a_{nn} (filled symbols) and a_{pp} (empty symbols) estimates including electromagnetic short-range effects. For the a_{nn} values: blue triangle from²⁹, green square from³⁰, orange circle from³¹, red line (upper bound of -18.3 fm at the 95% confidence level) from³², brown diamond from³³, purple circle from³⁴ and pink triangle from³⁵. For the a_{pp} values: black circle for⁵ and green square for¹⁰. Values from^{7,8,19} refer to a_{pp}^N values: orange downward triangle for¹⁹, red diamond for⁷, blue upward triangle for⁸. The horizontal light-blue and light-purple bands display the uncertainty of the current accepted short-range a_{nn} and a_{pp} values of -18.6 ± 0.4 ² and -17.6 ± 0.4 fm⁵, respectively. Light-green and light-pink bands refer to the current accepted a_{nn}^N and a_{pp}^N values of -18.9 ± 0.4 and -17.3 ± 0.4 fm respectively¹².

part of systematic uncertainty in the nuclear a_{pp} error budget²⁸. To frame the result in the context of recent literature, we make use of Fig. 6, similar to figure 1 of Ref. 2, where our newly obtained a_{pp} experimental (filled black triangle) and a_{nn}^{sr} (filled red rectangle) and a_{pp}^{sr} (empty red rectangle) model values are compared with recent a_{nn} (filled symbols) and a_{pp} (empty symbols) “short-range” estimates. The a_{nn} values are represented as blue triangle from²⁹, green square from³⁰, orange circle from³¹, red line (upper bound of -18.3 fm at the 95% confidence level) from³², brown diamond from³³, purple circle from³⁴ and pink triangle from³⁵. The a_{pp} values are given as black circle from⁵ and green square from¹⁰. Values from¹⁹ (empty orange downward triangle),⁷ (empty red diamond) and⁸ (empty blue upward triangle) refer to a_{pp}^N . Light-blue and light-purple bands display the uncertainty on the current accepted a_{nn} and a_{pp} short-range values of -18.6 ± 0.4 ² and -17.6 ± 0.4 fm⁵ respectively, obtained correcting the nuclear estimates for the electromagnetic effects. Light-green and light-pink bands refer to the current accepted a_{nn}^N and a_{pp}^N values of -18.9 ± 0.4 and -17.3 ± 0.4 fm respectively¹². We can observe that while literature estimates generally show large dispersion, our numbers appear more consistent with each other.

An important outcome of this work is that we can confirm the violation of the charge independence of nuclear forces, and suggest a lower charge symmetry breaking of nuclear forces as clearly displayed in Fig. 4.

Conclusions

We have exploited the quasi-free $p-p$ scattering below 1 MeV extracted from the ${}^2\text{H}(p, pp)n$ reaction using the THM to obtain the first experimental estimate of the Coulomb free 1S_0 $p-p$ scattering length and effective range. The success of our pivotal procedure relies on a basic feature of the reaction, namely the suppression of Coulomb effects in the extracted two-body cross

section at sub-Coulomb energies, as well as on the concept of universal window applicable to the NN system. Based on the idea that the NN phase shift δ in the conventional tool to analyze NN scattering data at low energies contains all short range effects and assisted by a model based on universality concepts that we have developed to help interpret the results, we conclude that this technique provides us with parameters to assess the charge symmetry breaking of the short-range interaction as a whole. This triggers the proposal of a new paradigm in the study of the charge symmetry breaking, in line with the current understanding that, at a fundamental level, the charge dependence of nuclear forces is due to a difference between the masses of the up and down quark and to electromagnetic interactions among the quarks.

Our results imply that the whole effect from the different up-down quark masses and residual electromagnetic properties has a smaller impact on the charge symmetry breaking, but still in the direction to help solve the Nolen-Schiffer anomaly for light nuclei¹, provided that different sources contribute. For example, binding energy differences are expected to receive more than 50% of their contribution from NN partial waves beyond 1S_0 ^{1,12} and can be partly explained with the inclusion of three-nucleon interactions³⁶; within the quark-meson coupling model proposed in³⁷, the difference between quark scalar densities in p and n generates an effective n - p mass difference of the right magnitude to add to the u - d quark mass difference.

Additional experimental and theoretical studies at low energies are urgently called for to better constrain the current existing models of charge symmetry breaking and Coulomb corrections filling up our basic understanding of low-energy NN scattering. A decisive experimental contribution would be a more precise determination of a_{nn} . In this regard, the approach here presented will play a key role in the next future and opens to the possibility to access the n - n scattering cross section by measuring the quasi-free $n + d \rightarrow n + n + p$ reaction.

Methods

THM basic features. The THM has its background in the theory of direct reactions and in particular in the studies of the QF reaction mechanisms^{16,17}. It is considered as a transfer to the continuum with the TH nucleus a that breaks up into x , the transferred nucleus, and s , the spectator to the $A(x,b)B$ reaction. This process contributes to the cross section in the three-body phase space where the momentum transfer to the spectator s is small. This is called QF kinematics regime. As the transferred nucleus x is virtual, its energy and momentum are not linked by the usual energy-momentum relation for a free particle. This gives to the $A(x,b)B$ reaction its half-off-the-energy-shell character. The $A + a$ relative motion takes place at an energy above the Coulomb barrier ensuring that the transfer of particle x occurs inside the nuclear field of A without undergoing Coulomb suppression or electron screening. However, the $A + x$ reaction takes place at sub-Coulomb relative energy $E_{c.m.}$ since the excess of energy in the $A + a$ relative motion is needed for the break-up of the TH nucleus $a = (xs)$. From energy and momentum conservation principles, one obtains:

$$E_{c.m.} = \frac{m_x}{m_x + m_A} E_A - \frac{p_s^2}{2\mu_{sF}} + \frac{\vec{p}_s \cdot \vec{p}_A}{m_x + m_A} - B_{xs}, \tag{6}$$

with m_i and \vec{p}_i , the mass and momentum of particle i , $\mu_{ij} = m_i m_j / (m_i + m_j)$ the reduced mass of particles i and j ($F = A + x = b + B$) and $F_{xs} = m_x + m_s - m_a$ the binding energy of clusters x and s inside a . $E_{c.m.}$ can vary within a range determined by the momentum of the spectator particle, p_s and/or its emission angle. As for p_s , its values should not overcome the theoretical upper limit for the relative momentum p_{xs} between x and s (in the laboratory system $\vec{p}_{xs} = \vec{p}_x = -\vec{p}_s$) represented by the OES bound state wave number $\kappa_{xs} = \sqrt{2\mu_{xs} B_{xs}}$. For the $d = p \oplus n$ system, $\kappa_{xs} = 45.5$ MeV/c, absolutely consistent with the choice to select events with p_s values lower than 20 MeV/c to determine the HOES $p - p$ scattering cross section in^{13,14}.

In PWIA, the three body reaction can be factorized into two terms and given by:

$$\frac{d^3\sigma}{d\Omega_B d\Omega_b dE_B} = (KF) \cdot |\phi(p_{xs})|^2 \cdot \left[\frac{d^2\sigma_{xA \rightarrow bB}}{dE_{c.m.} d\Omega} \right]^{HOES}, \tag{7}$$

clearly showing their close connection. In the equation, KF is a kinematical factor containing the final state phase space factor and it is a function of the masses, momenta, and angles of the outgoing particles¹⁷; $|\phi(p_{xs})|^2$ is the Fourier transform of the radial wave function for the $\chi(r_{xs})$ inter-cluster motion whose functional dependence is fixed by xs system properties; $d^2\sigma_{xA \rightarrow bB}/dE_{c.m.} d\Omega^{HOES}$ is the HOES differential cross section for the binary $A(x,b)B$ reaction at the $E_{c.m.}$ center of mass energy.

A proof of validity of the PWIA and thus of the previous factorization is the agreement between the shapes of the theoretical and experimental momentum distributions of particle s . Refers to^{13,14} for further details. This agreement is a proof of existence and dominance of the QF mechanism, and rules out within experimental errors any contribution from higher order terms and three-body forces. This result is consistent with the conclusions of³⁸⁻⁴⁰, where these contributions have been investigated in various situations and energies. The THM has been applied to several reactions of astrophysical interest. See⁴¹⁻⁴⁵ for recent applications.

Effective field theory concepts. The interaction between nucleons is a residual interaction of QCD in the low energy regime. In recent years, this interaction has been obtained by a perturbative series using an Effective Field Theory (EFT) having the symmetries of QCD. Extending this approach to describe the physics inside the universal window, a model-independent description is given using an EFT based on the separation of scales produced by the typical momentum of the system, of the order of $1/a$, and the underlying high momentum scale, of the order of $1/l$. In nuclear physics this approach is known as pionless-EFT¹⁵. Its lowest orders are equivalent to the effective range expansion of the s -wave phase shift given in Eq. (2) of the main text.

It should be noticed that inside the universal window the effective range expansion and its extension to describe the negative energy pole, Eqs. (2) and (4), introduce a strict correlation between the low energy parameters responsible for the appearance of the universal behavior. When both equations are simultaneously verified at a confident level the dynamics of two-body systems is highly independent of the details of the particle interaction. This property can be exploited to characterize the universal window by a general Gaussian potential²⁷:

$$V(r) = V_0 e^{-r^2/r_0^2}, \tag{8}$$

with r the inter-particle distance. For each system, the strength V_0 and the range r_0 are modulated in order to reproduce the experimental scattering length and the effective range values. We can consider this potential a low-energy representation of the two-particle interaction since it is able to accurately describe the low-energy behavior of the system. In the present work, we exploit this characteristic to estimate the $p - p$ Coulomb-free scattering length.

To show how the universal concepts can be exploited in the present context, we first illustrate the model independence of the procedure used in the present study. To this aim, the scattering length and effective range values calculated using the Argonne v_{18} NN potential²⁵, shown in Table 2 for the nn and pp case, are used as reference values. The Argonne v_{18} potential includes explicitly the electromagnetic part v^{EM} . This potential includes several contributions as vacuum polarization, two photon exchange and magnetic moment interactions. Moreover, its short-range part is regularized using dipole nucleon form factors. Accordingly, there are two

Table 2 The effect of electromagnetic terms. Low-energy parameters with and without the inclusion of the electromagnetic terms for the two potential models indicated.

	Argonne v_{18}	w/o v^{EM}	Argonne v_{18}	w/o v^{EM}
$^1a_{nn}(\text{fm})$	-18.487	-18.818	$^1a_{pp}(\text{fm})$	-7.806
$^1r_{nn}(\text{fm})$	2.840	2.834	$^1r_{pp}(\text{fm})$	2.788
	Gaussian	w/o v^{EM}	Gaussian	w/o v^{EM}
$^1a_{nn}(\text{fm})$	-18.487	-18.89 ± 0.02	$^1a_{pp}(\text{fm})$	-7.806
$^1r_{nn}(\text{fm})$	2.85 ± 0.07	2.83 ± 0.07	$^1r_{pp}(\text{fm})$	2.77 ± 0.08
				-17.19 ± 0.03
				2.86 ± 0.08

contributions to the short-range physics coming from the strong part of the AV18 interaction and from v^{EM} . The electromagnetic effects usually are estimated by calculating the zero-range parameters without including this part. These results are shown in the third and sixth column of the table. We now use the Gaussian potential, supplemented by including v^{EM} , and fix the strength V_0 and range r_G in order to describe the corresponding Argonne v_{18} values. The quality of the agreement is shown in the second and fourth columns where we have considered Gaussian ranges inside the interval $r_G = 1.85 \pm 0.05$ fm. This variation on the Gaussian range produces some variation on the $^1r_{nn}$ and $^1r_{pp}$ values, as indicated in the Table. Once the strength of the Gaussian potential is fixed, we can calculate the corresponding zero-energy quantities without the inclusion of v^{EM} . The results are shown in the third and sixth column and, as we can see from the Table, the Gaussian interaction reproduces the nuclear Argonne v_{18} values (without including v^{EM}) within a 0.5% accuracy which is a remarkable result. So, using this simple model we have shown that details to the specific form of the potential are not important. The dynamics is governed by the long-range behavior, a manifestation of universal behavior.

Bayesian analysis approach. Bayesian data-fitting is an approach to data analysis based on Bayes theorem, where the background knowledge on the parameters of the chosen model is updated with the information from the observed data⁴⁶. This background knowledge is expressed as a prior distribution and combined with observed data using a likelihood function to determine the posterior distribution. Therefore, the Bayesian approach uses probability to describe what is known about the parameters. In this framework, the posterior distribution function of the parameters Θ , given the data D , is given by the formula:

$$p(\Theta|D) = \frac{p(D|\Theta)p(\Theta)}{p(D)}, \quad (9)$$

where $p(D|\Theta)$ is the likelihood function of the data D , given the parameters Θ , $p(\Theta)$ is the prior distribution function of Θ and $p(D)$ is the so-called model evidence, which is a normalization factor usually neglected in the calculation since it is difficult to compute. To sample the posterior distributions in real situations where probabilistic inference is used, Markov Chain Monte Carlo (MCMC) methods are usually applied. Indeed, MCMC methods can be used even without a full analytic description of the aforementioned probability distributions and do not necessarily require computing any process-intensive task such as calculating derivatives or integrals of the function. Many of the MCMC applications use the Metropolis–Hasting (M–H) method⁴⁷ to generate the chain, however, this algorithm is very sensitive to a set of “tuning” parameters, the number of which scales with the square of the dimension of the parameters space. Several heuristic methods have been developed to estimate these tuning parameters in a data-driven fashion. In particular, we decided to use the *emcee*²³ Python library which is based on the algorithm described in²⁴ and has been thoroughly used in astrophysics.

Data availability

All relevant data are available from the corresponding author on reasonable request.

Received: 20 May 2022; Accepted: 26 April 2023;

Published online: 18 May 2023

References

1. Miller, G. A., Opper, A. K. & Stephenson, E. J. Charge symmetry breaking and QCD. *Annu. Rev. Nucl. Part. Sci.* **56**, 253 (2006).
2. Goebel, M. et al. Neutron-neutron scattering length from the $^6\text{He}(p,p\alpha)nn$ reaction. *Phys. Rev. C* **104**, 024001 (2021).
3. Piarulli, M. et al. Local chiral potentials and the structure of light nuclei. *Phys. Rev. C* **91**, 024003 (2015).
4. Kok, L. P. Accurate determination of the ground-state level of the ^2He nucleus. *Phys. Rev. Lett.* **45**, 427 (1980).
5. Alberverio, S., Ferreira, L. S., Gesztesy, F., Hoegh-Krohn, R. & Streit, L. Model dependence of Coulomb-corrected scattering lengths. *Phys. Rev. C* **29**, 680 (1984).
6. Rahman, M. & Miller, G. A. Model dependence of the 1S_0 pp scattering length. *Phys. Rev. C* **27**, 917 (1983).
7. Kong, X. & Ravnal, F. Proton-proton scattering lengths from effective field theory. *Phys. Lett. B* **450**, 320 (1999).
8. Ando, S. I., Shin, J. W., Hyun, C. H. & Hong, S. W. Low energy proton-proton scattering in effective field theory. *Phys. Rev. C* **76**, 064001 (2007).
9. Kaplan, D. B., Savage, M. J. & Wise, M. B. Perturbative calculation of the electromagnetic form factors of the deuteron. *Phys. Rev. C* **59**, 617 (1999).
10. Walz, M., Meißner, U.-G. & Epelbaum, E. Charge-dependent nucleon-nucleon potential from chiral effective field theory. *Nucl. Phys. A* **693**, 663 (2001).
11. Epelbaum, E., Gloeckle, W. & Meißner, G. The two-nucleon system at next-to-next-to-next-to-leading order. *Nucl. Phys. A* **747**, 362 (2005).
12. Machleidt, R. & Slaus, I. The nucleon-nucleon interaction. *J. Phys. G* **27**, R69 (2001).
13. Tumino, A. et al. Suppression of the Coulomb Interaction in the Off-Energy-Shell $p-p$ Scattering from the $p+d \rightarrow p+p+n$ Reaction. *Phys. Rev. Lett.* **98**, 252502 (2007).
14. Tumino, A. et al. Off-energy-shell $p-p$ scattering at sub-Coulomb energies via the Trojan horse method. *Phys. Rev. C* **78**, 064001 (2008).
15. Hammer, H.-W., König, S. & van Kolck, U. Nuclear effective field theory: status and perspectives. *Rev. Mod. Phys.* **92**, 025004 (2020).
16. Pizzone, R. G. et al. Clusters and their fundamental role for Trojan Horse Method. *Eur. Phys. J. A* **56**, 283 (2020).
17. Tumino, A. et al. The Trojan Horse Method: a nuclear physics tool for astrophysics. *Ann. Rev. Nucl. Particle Sci.* **71**, <https://doi.org/10.1146/annurev-nucl-102419-033642> (2021).
18. Slaus, I. et al. Quasifree processes in the $^2\text{H} + ^3\text{He}$ interaction. *Nucl. Phys. A* **286**, 67 (1977).
19. Miller, G. A. et al. Charge symmetry, quarks and mesons. *Phys. Rep.* **194**, 1 (1990).
20. Blatt, J. M. & Jackson, J. D. On the interpretation of neutron-proton scattering data by the schwinger variational method. *Phys. Rev.* **76**, 18 (1949).
21. Bethe, H. A. Theory of the effective range in nuclear scattering. *Phys. Rev.* **76**, 38 (1949).
22. Babenko, V. A. & Petrov, N. M. Determination of low-energy parameters of neutron-proton scattering in the the shape-parameter approximation from present-day experimental data. *Phys. Atom. Nucl.* **73**, 1499 (2010).
23. Foreman-Mackey, D., Hogg, D. W., Lang, D. & Goodman, J. The MCMC hammer. *Publ. Astron. Soc. Pac.* **125**, 306 (2013).
24. Goodman, J. & Weare, J. Ensemble samplers with affine invariance. *Math. Comput. Sci. J.* **5**, 6580 (2010).
25. Wiringa, R. B., Stoks, V. G. J. & Schiavilla, R. Accurate nucleon-nucleon potential with charge-independence breaking. *Phys. Rev. C* **51**, 38 (1995).
26. Braaten, E. & Hammer, H.-W. Universality in few-body systems with large scattering length. *Phys. Rep.* **428**, 259 (2006).
27. Kievsky, A., Gattobigio, M., Girlanda, L. & Viviani, M. Efimov physics and connections to nuclear physics. *Annu. Rev. Nucl. Particle Sci.* **71**, 465 (2021).
28. Nakamura, S. X., Ishikawa, T. & Sato, T. Neutron-neutron scattering length from π^+ photoproduction on the deuteron. arXiv: 2003.02497 (2020).
29. Howell, C. R. et al. Toward a resolution of the neutron-neutron scattering-length issue. *Phys. Lett. B* **444**, 252 (1998).
30. Huhn, V. et al. New investigation of the neutron-neutron and neutron-proton final-state interaction in the n-d breakup reaction. *Phys. Rev. C* **63**, 014003 (2001).
31. Gonzalez Trotter, D. E. et al. New Measurement of the 1S_0 neutron-neutron scattering length using the neutron-proton scattering length as a standard. *Phys. Rev. Lett.* **83**, 3788 (1999).
32. Baumer, C. et al. Measurement of the $^2\text{H}(d,^2\text{He})^2n$ reaction at $E_d = 171$ MeV and implications for the neutron-neutron scattering length. *Phys. Rev. C* **71**, 044003 (2005).
33. VonWitsch, W., Ruan, X. & Witala, H. Neutron-neutron final-state interaction in the $^2\text{H}(n,p)^2n$ reaction at $E_n = 17.4$ MeV. *Phys. Rev. C* **74**, 014001 (2006).
34. Gonzalez Trotter, D. E. et al. Neutron-deuteron breakup experiment at $E_n = 13$ MeV: determination of the 1S_0 neutron-neutron scattering length a_{nn} . *Phys. Rev. C* **73**, 034001 (2006).
35. Chen, Q. et al. Measurement of the neutron-neutron scattering length using the π^-d capture reaction. *Phys. Rev. C* **77**, 054002 (2008).
36. Nogga, A. et al. Three-nucleon bound states using realistic potential models. *Phys. Rev. C* **67**, 034004 (2003).
37. Saito, K. & Thomas, A. W. A quark-meson coupling model for nuclear and neutron matter. *Phys. Lett. B* **335**, 17 (1994).
38. Šlaus, I., Akaishi, Y. & Tanaka, H. Neutron-neutron effective range parameters. *Phys. Rep.* **173**, 257 (1989).
39. Witala, H., Golak, J., Skibiński, R., Soloviev, V. & Topolnicki, K. Three-nucleon force effects in inclusive spectra of the neutron-deuteron breakup reaction. *Phys. Rev. C* **101**, 054002 (2020).
40. Maris, P. et al. LENPIC Collaboration. Nuclear properties with semilocal momentum-space regularized chiral interactions beyond N2 LO. *Phys. Rev. C* **106**, 064002 (2020).
41. Tumino, A. et al. An increase in the $^{12}\text{C} + ^{12}\text{C}$ fusion rate from resonances at astrophysical energies. *Nature* **557**, 687–690 (2018).
42. Lania, L. et al. Cross-section measurement of the cosmologically relevant $^7\text{Be}(n,\alpha)^4\text{He}$ reaction over a broad energy range in a single experiment. *Astrophys. J.* **879**, 23 (2019).
43. Pizzone, R. G. et al. Indirect measurement of the $^3\text{He}(n,p)^3\text{H}$ reaction cross section at Big Bang energies. *Euro. Phys. J. A* **56**, 199 (2020).

44. Hayakawa, S. et al. Constraining the primordial lithium abundance: new cross section measurement of the ${}^7\text{Be}+n$ reactions updates the total ${}^7\text{Be}$ destruction rate. *Astrophys. J. Lett.* **915**, L13 (2021).
45. La Cognata, M. et al. Exploring the astrophysical energy range of the ${}^{27}\text{Al}(p,\alpha){}^{24}\text{Mg}$ reaction: a new recommended reaction rate. *Phys. Lett. B* **826**, 136917 (2022).
46. van de Schoot, R. et al. Bayesian statistics and modelling. *Nat. Rev. Methods Primers* **1**, 1 (2021).
47. Hastings, W. K. Monte carlo sampling methods using Markov chains and their applications. *Biometrika* **57**, 97109 (1970).

Acknowledgements

The authors wish to thank prof. R. Schiavilla for fruitful discussions. A.O. acknowledges the support of dr. R.J. deBoer for Bayesian fitting analysis. C.A.B. was supported as a HFHF Visiting Professor of the German Helmholtz Research Academy and by the U.S. DOE grant DE-FG02-08ER41533. L.L., S.R. and M.L.S. acknowledge “Programma ricerca di ateneo UNICT 2020-22 linea2” and “Starting grant 2020” of University of Catania. A.O. acknowledges support by the National Science Foundation under Grant No. OISE-1927130 (IReNA).

Author contributions

A.T., G.G.R. and M.L.C. conceived the idea of the project. A.T. performed the data analysis. G.G.R. and M.L.C. assisted with the data analysis. A.O. performed the Bayesian fit. A.T., G.G.R. and D.L. assisted with the fitting procedure. A.K., M.G. and M.V. performed model calculations. A.T. interpreted the results and wrote the manuscript. A.T., M.L.C. and A.O. prepared the figures. G.G.R., M.L.C. and A.K. assisted with the manuscript preparation and interpretation of the results. C.A.B., G.D., M.G., G.L.G., L.L., D.L., R.G.P., S.R., M.L.S., R.S., and M.V. contributed to the interpretation of the results and revised the manuscript.

Competing interests

The authors declare no competing interests.

Additional information

Correspondence and requests for materials should be addressed to Aurora Tumino.

Peer review information *Communications Physics* thanks Jack Bishop and the other, anonymous, reviewer(s) for their contribution to the peer review of this work.

Reprints and permission information is available at <http://www.nature.com/reprints>

Publisher's note Springer Nature remains neutral with regard to jurisdictional claims in published maps and institutional affiliations.



Open Access This article is licensed under a Creative Commons Attribution 4.0 International License, which permits use, sharing, adaptation, distribution and reproduction in any medium or format, as long as you give appropriate credit to the original author(s) and the source, provide a link to the Creative Commons license, and indicate if changes were made. The images or other third party material in this article are included in the article's Creative Commons license, unless indicated otherwise in a credit line to the material. If material is not included in the article's Creative Commons license and your intended use is not permitted by statutory regulation or exceeds the permitted use, you will need to obtain permission directly from the copyright holder. To view a copy of this license, visit <http://creativecommons.org/licenses/by/4.0/>.

© The Author(s) 2023